

Interference of locally excited surface plasmons

L. Novotny^{a)}

Swiss Federal Institute of Technology, ETH Zürich, CH-8092 Zürich, Switzerland

B. Hecht and D. W. Pohl

IBM Research Division, Zurich Research Laboratory, CH-8803 Rüschlikon, Switzerland

(Received 25 September 1996; accepted 5 November 1996)

Surface plasmon interactions on a finite silver layer are theoretically investigated using a coupled dipole formalism. The studied system consists of several protruding particles located on the surface of the layer that are scanned with an optical probe. An optical scan-image of the silver surface is obtained by assigning the recorded far-field radiation to the momentary position of the optical probe. Both, probe and protrusions are considered as single dipolar particles. Interferences of the locally excited surface plasmons can be recorded by detecting the radiation emitted into the lower half-space at angles beyond the critical angle of total internal reflection (forbidden light). The resulting scan images show excellent agreement with recent experimental measurements. The theory of the coupled dipole formalism using Green's functions of a layered reference system is outlined and electromagnetic properties of surface plasmons are discussed. © 1997 American Institute of Physics. [S0021-8979(97)01804-5]

I. INTRODUCTION

By definition surface plasmons are the quanta of surface-charge-density oscillations,¹ but the same terminology is commonly used for collective oscillations in the electron density at the surface of a metal. In the past, surface plasmons have attracted considerable attention due to their application to optical sensor devices.²⁻⁴ The first experiments on surface plasmons were carried out with electron-energy-loss measurements.⁵⁻⁹ Later it was found, that the same measurements can be accomplished with supercritical light excitation in the famous Otto or Kretschmann configuration,⁹⁻¹² and the technique is known as the attenuated total reflection technique (ATR). The theory of optically excited surface plasmons can be well described by macroscopic electrodynamic theory, as long as the mean free path of the electrons in the metal is much shorter than the wavelength of the plasmons.¹³ At optical frequencies this condition is approximately fulfilled, because the finite losses of metals limit the minimum plasmon wavelength to about one third of the incident radiation.¹⁴ However, for certain aspects nonlocal, hydrodynamic theories might be more appropriate.² From a macroscopic electrodynamic point of view, surface plasmons are a type of surface waves, i.e., waves that propagate along metal surfaces and which decay in normal direction from the surfaces. A comprehensive discussion of surface plasmons and corresponding experimental techniques are given by Raether.⁹

The aim of this paper is to understand plasmon generation by local excitations and to study electrodynamic interactions on a finite metal layer. The interactions between metal particles and a metal surface have been investigated both experimentally¹⁵⁻¹⁷ and theoretically.¹⁸⁻²⁴ Many theoretical treatments are done in the quasi-static limit, by reducing the complexity to two dimensions, or by neglecting re-

tardation in Green's dyadic functions. Furthermore, the investigations are often restricted to the phenomenological analysis of the configurational resonances in the system. The present study aims towards a more or less complete and self-consistent analysis. Of special interest are near and long range interactions on the surface of a metal layer and the coupling mechanisms to far-field radiation. It will be shown, that the theoretical results are in excellent agreement with recent experiments.

The system that is studied consists of a silver layer that is deposited on a glass substrate having a frequency independent dielectric constant $\epsilon_n = 2.25$ [Fig. 1]. Protrusions on the silver layer are considered as small, dipolar silver particles of variable size. Another dipolar particle is used as a tiny light emitting optical probe that is raster scanned over the surface of the layer at constant height, similar to the experimental situation in aperture scanning near-field optical microscopy (aperture SNOM).²⁵⁻²⁸ The probing particle is locally excited by the monochromatic field \mathbf{E}_o . An optical scan image of the surface of the silver layer is obtained by recording the far-field radiation for every position (x,y) of the optical probe.

II. THEORY

It is assumed that the exciting electric field \mathbf{E}_o is harmonic in time and that the layered media and the particles are linear, isotropic and non-magnetic ($\mu = 1$). In this case, the total electric field $\mathbf{E}(\mathbf{r},t)$ is also time harmonic, but the factor $\exp(-i\omega t)$ will be suppressed. The dielectric information of the entire system can be represented by a spatially inhomogeneous dielectric constant $\epsilon(\mathbf{r})$. It is convenient to describe the dielectric constant of the planarly layered reference frame by $\epsilon_{ref}(\mathbf{r})$. Then, $[\epsilon(\mathbf{r}) - \epsilon_{ref}(\mathbf{r})]$ defines the dielectric response of the particles relative to the layered reference system.

In the absence of source currents and charges and with the conditions stated above, Maxwell's curl equations read

^{a)}Present address: Pacific Northwest National Laboratory, P.O. Box 999, Richland, WA 99352. Electronic mail: l_novotny@pnl.gov

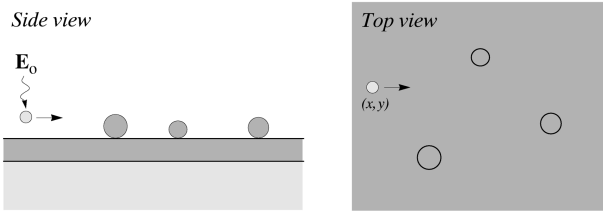


FIG. 1. Investigation of surface plasmon interactions with a four-particle model. Particle A ($\epsilon=2.25$, $a=5$ nm) represents the optical probe which is scanned over the particles B ($\epsilon=-9.13+0.31i$, $a=25$ nm), C ($\epsilon=-9.13+0.31i$, $a=20$ nm) and D ($\epsilon=-9.13+0.31i$, $a=15$ nm). Particle A is scanned at a constant height of 10 nm (surface to center of particle) and is excited by a local horizontal electric field \mathbf{E}_o at $\lambda=488$ nm. Particles B, C, and D are located on the surface of the layer. Silver layer: $\epsilon=-9.13+0.31i$, $d=50$ nm; upper half-space: $\epsilon_1=1$; lower half-space: $\epsilon_n=2.25$.

$$\nabla \times \mathbf{E}(\mathbf{r}) = i\omega\mu_o\mathbf{H}(\mathbf{r}) \quad (2.1)$$

$$\nabla \times \mathbf{H}(\mathbf{r}) = -i\omega\epsilon_o\epsilon_{ref}(\mathbf{r})\mathbf{E}(\mathbf{r}) + \mathbf{j}_e(\mathbf{r}), \quad (2.2)$$

where, according to the volume equivalence theorem,²⁹ \mathbf{j}_e is the volume distribution of the electric current density induced in the particles

$$\mathbf{j}_e(\mathbf{r}) = -i\omega\epsilon_o[\epsilon(\mathbf{r}) - \epsilon_{ref}(\mathbf{r})]\mathbf{E}(\mathbf{r}). \quad (2.3)$$

From Eqs. (2.1) and (2.2) it follows that \mathbf{E} has to fulfill the inhomogeneous wave equation

$$\nabla \times \nabla \times \mathbf{E}(\mathbf{r}) - k_o^2\epsilon_{ref}(\mathbf{r})\mathbf{E}(\mathbf{r}) = i\omega\mu_o\mathbf{j}_e(\mathbf{r}), \quad (2.4)$$

where the free space wavenumber k_o is equal to ω/c . The corresponding definition of the dyadic Green's function of the layered reference system reads³⁰

$$\nabla \times \nabla \times \tilde{\mathbf{G}}(\mathbf{r}, \mathbf{r}') - k_o^2\epsilon_{ref}(\mathbf{r})\tilde{\mathbf{G}}(\mathbf{r}, \mathbf{r}') = \tilde{\mathbf{I}}\delta(\mathbf{r} - \mathbf{r}'). \quad (2.5)$$

The vector \mathbf{r}' denotes the location of the point source and $\tilde{\mathbf{I}}$ is the unit dyadic. For later purpose it will be convenient to split $\tilde{\mathbf{G}}$ into two separate contributions

$$\tilde{\mathbf{G}}(\mathbf{r}, \mathbf{r}') = \tilde{\mathbf{G}}_o(\mathbf{r}, \mathbf{r}') + \tilde{\mathbf{G}}_s(\mathbf{r}, \mathbf{r}'). \quad (2.6)$$

$\tilde{\mathbf{G}}_s$ is the scattering part of Green's function and accounts for the secondary electromagnetic field, i.e., the field that is scattered by the layered system. $\tilde{\mathbf{G}}_o$ is the primary part of Green's function and contributes only to the field in the upper half-space. While the primary part $\tilde{\mathbf{G}}_o$ is analytically known, the scattering part $\tilde{\mathbf{G}}_s$ involves numerical integrations [c.f. Appendix A]. However, in the very near-field where retardation can be neglected, analytical solutions can be derived by the image dipole method.³¹ Analytical solutions can also be determined for the asymptotic far-fields.

As long as the fields are considered outside of the volume V occupied by the particles, the solution to Eq. (2.4) can be expressed in terms of the dyadic Green's function $\tilde{\mathbf{G}}$ as

$$\mathbf{E}(\mathbf{r}) = \mathbf{E}_o(\mathbf{r}) + i\omega\mu_o \int_V dV' \tilde{\mathbf{G}}(\mathbf{r}, \mathbf{r}') \mathbf{j}_e(\mathbf{r}') \quad \mathbf{r} \notin V, \quad (2.7)$$

where V' indicates that the volume integration refers to the variable \mathbf{r}' . \mathbf{E}_o denotes the homogeneous solution ($\mathbf{j}_e=0$ everywhere), i.e., the solution in the absence of the particles

and corresponds in the present situation to the local exciting field. Eq. (2.7) together with the electric current density Eq. (2.3) define an implicit integral equation for the unknown field \mathbf{E} (Fredholm equation of the second kind).

In deriving the volume integral equation, it has been assumed that the operator $\nabla \times \nabla \times$ may be interchanged with the volume integration. This assumption is not strictly valid and special care must be applied if the fields are to be evaluated in the source region ($\mathbf{r} \in V$). To be strictly correct, an infinitesimal exclusion volume surrounding $\mathbf{r}=\mathbf{r}'$ has to be introduced (*principal volume*) excluding the singularity of $\tilde{\mathbf{G}}$ at $\mathbf{r}=\mathbf{r}'$.^{32,33} Depolarization of the principal volume must be treated separately which results in an additional term ($\tilde{\mathbf{L}}$) depending on the geometrical shape of the volume. Furthermore, in numerical schemes the principal volume has a finite size giving rise to a second correction term $\tilde{\mathbf{M}}$.

The particles can be regarded as single dipoles as long as their size is considerably smaller than the interior wavelength and smaller than the skin depth. Larger particles have to be subdivided into a number of dipolar subvolumes. However, the focus of this study is on dipolar particles only. In this case, the electric current density \mathbf{j}_e can be expressed in terms of the individual dipole moments as

$$\mathbf{j}_e(\mathbf{r}) = -i\omega \sum_{n=1}^N \mathbf{p}_n \delta(\mathbf{r} - \mathbf{r}_n). \quad (2.8)$$

The dipole moment \mathbf{p}_n of the particle at $\mathbf{r}=\mathbf{r}_n$ is proportional to the *exciting* electric field $\mathbf{E}_{exc}(\mathbf{r}_n)$ according to

$$\mathbf{p}_n = \tilde{\alpha}_n \mathbf{E}_{exc}(\mathbf{r}_n), \quad (2.9)$$

where $\tilde{\alpha}_n$ is the polarizability of the n -th particle. It has to be emphasized that $\mathbf{E}_{exc}(\mathbf{r}_n)$ is generally not equal to the field $\mathbf{E}(\mathbf{r}_n)$ that is actually present at a given point \mathbf{r}_n ! $\mathbf{E}_{exc}(\mathbf{r}_n)$ is the field that arrives at \mathbf{r}_n generated by other dipoles and inhomogeneities ($\tilde{\mathbf{G}}_s$) in the environment. However, for simpler notation, the subscript *exc* will be ignored in the following. The reader has to keep in mind, that the field only represents the actual field at points outside the particles.

After inserting Eqs. (2.9), (2.8) into the volume integral equation Eq. (2.7), evaluating the resulting field at the position \mathbf{r}_k of the subvolume V_k , and multiplying both sides with $\tilde{\alpha}_k$, we obtain a system of equations for the unknown dipole moments

$$\mathbf{p}_k = \tilde{\alpha}_k \mathbf{E}_o(\mathbf{r}_k) + \omega^2 \mu_o \tilde{\alpha}_k \tilde{\mathbf{G}}_s(\mathbf{r}_k, \mathbf{r}_k) \mathbf{p}_k + \omega^2 \mu_o \sum_{\substack{n=1 \\ n \neq k}}^N \tilde{\alpha}_k \tilde{\mathbf{G}}_s(\mathbf{r}_k, \mathbf{r}_n) \mathbf{p}_n, \quad k=1, \dots, N. \quad (2.10)$$

Since every equation is a vector equation the above system defines a $3N \times 3N$ matrix equation which has to be solved numerically. Once the dipole moments are determined the electric field can be evaluated at any *exterior* point \mathbf{r} according to

$$\mathbf{E}(\mathbf{r}) = \mathbf{E}_o(\mathbf{r}) + \omega^2 \mu_o \sum_{n=1}^N \tilde{\mathbf{G}}(\mathbf{r}, \mathbf{r}_n) \mathbf{p}_n \quad \mathbf{r} \notin V. \quad (2.11)$$

The solutions for the actual field inside V are beyond the scope of this paper. The interested reader is referred to the paper by Lakhtakia.³⁴

In order to solve the system of equations Eq. (2.10), explicit expressions for the polarizabilities $\vec{\alpha}_k$ are required. The exact expressions for $\vec{\alpha}_k$ can be derived from the equivalence of the coupled dipole method and the method of moments as³⁴

$$\vec{\alpha}_k = \left(4\pi a_k^3 \varepsilon_o \varepsilon_1 \frac{\varepsilon(\mathbf{r}_k) - \varepsilon_1}{\varepsilon(\mathbf{r}_k) + 2\varepsilon_1} \right) \times \left(\vec{\mathbf{I}} - 3k_1^2 \frac{\varepsilon(\mathbf{r}_k) - \varepsilon_1}{\varepsilon(\mathbf{r}_k) + 2\varepsilon_1} \vec{\mathbf{M}}(\mathbf{r}_k) \right)^{-1}, \quad (2.12)$$

where the dyadic $\vec{\mathbf{M}}$ is given by

$$\vec{\mathbf{M}}(\mathbf{r}_k) = \frac{2}{3} \frac{1}{k_1^2} [[1 - ik_1 a_k] \exp[ik_1 a_k] - 1] \vec{\mathbf{I}}. \quad (2.13)$$

$\vec{\mathbf{I}}$ represents the unit dyadic and $\varepsilon(\mathbf{r}_k)$ denotes the dielectric constant of the k -th particle with radius a_k . The particle is assumed to be located in the upper half-space characterized by the dielectric constant ε_1 and the wavenumber $k_1 = (\omega/c)\sqrt{\varepsilon_1}$. The dyadic $\vec{\mathbf{M}}$ accounts for the finite size of the particle. In the limit $a_k \rightarrow 0$, $\vec{\mathbf{M}}$ equals zero and $\vec{\alpha}_k$ reduces to the electrostatic polarizability of a small sphere derivable from the Clausius–Mosotti relation.³⁵ In order to fulfill the optical theorem and therefore to arrive at physical solutions, the inclusion of $\vec{\mathbf{M}}$ in the expression (2.12) is essential even for small particles. As discussed by Lakhtakia,³⁴ a series expansion of $\vec{\mathbf{M}}$ renders the radiation reaction term obtained by Draine.³⁶

A. Far-field radiation

The individual particles scatter *coherently*, i.e., the phases of the induced dipole moments are proportional to the phase of the incident radiation. In order to determine the radiation patterns of the ensemble, explicit expressions for the asymptotic far-fields are needed.

The flux of radiation corresponds to the time-averaged Poynting vector $\langle \mathbf{S} \rangle$. Since in the far-field the electromagnetic field is purely transverse, $\langle \mathbf{S} \rangle$ has only a radial component, making a representation in spherical coordinates advantageous. In this system, the angular power density $p(\vartheta, \varphi)$ is defined as the power radiated into the solid angle $d\Omega = \sin\vartheta d\vartheta d\varphi$, and the power P radiated into $\Delta\Omega = (\Delta\vartheta, \Delta\varphi)$ reads

$$P(\Delta\Omega) = \int_{\Delta\varphi} d\varphi \int_{\Delta\vartheta} d\vartheta \sin\vartheta p(\vartheta, \varphi). \quad (2.14)$$

$p(\vartheta, \varphi)$ corresponds to the flux of $\langle \mathbf{S} \rangle$ through a surface element $da = |\mathbf{r}|^2 d\Omega$ with $|\mathbf{r}|$ being the radial distance. Thus,

$$p(\vartheta, \varphi) = |\mathbf{r}|^2 \langle \mathbf{S} \rangle \cdot \mathbf{n}_r, \quad (2.15)$$

where \mathbf{n}_r is the unit vector in radial direction. In the far-field, the fields \mathbf{E} and \mathbf{H} are transverse, have identical phases, and a definite amplitude ratio given by the wave impedance. Therefore, $\langle \mathbf{S} \rangle$ can be expressed in terms of \mathbf{E} alone

$$\langle \mathbf{S} \rangle = \frac{1}{2} \text{Re} \{ \mathbf{E} \times \mathbf{H}^* \} = \frac{1}{2} \sqrt{\frac{\varepsilon_o \varepsilon_j}{\mu_o}} |\mathbf{E}|^2 \mathbf{n}_r. \quad (2.16)$$

The index j specifies the domain in which the fields have to be evaluated. The field \mathbf{E} of a system of N dipoles is given by Eq. (2.11). To evaluate this equation in the far-field, an asymptotic form for the Green's function has to be determined. These asymptotic forms can be derived by using the method of steepest descents; explicit expressions are given in Ref. 37. It is important to treat the primary part $\vec{\mathbf{G}}_o$ and the scattering part $\vec{\mathbf{G}}_s$ of $\vec{\mathbf{G}}$ separately since they contribute independently to the fields. Since all particles are located in the upper half-space, the primary part vanishes everywhere except in the upper half-space.

It can be shown, that the factor $\exp(ik_j |\mathbf{r}|)/|\mathbf{r}|$ can be extracted out of the asymptotic expressions for $\vec{\mathbf{G}}_o$ and $\vec{\mathbf{G}}_s$

$$\lim_{|\mathbf{r}| \rightarrow \infty} \vec{\mathbf{G}}_o(\mathbf{r}, \mathbf{r}_k) = \frac{\exp(ik_j |\mathbf{r}|)}{|\mathbf{r}|} \vec{\mathbf{G}}_o^\infty(\mathbf{r}_k, \mathbf{n}_r), \quad (2.17)$$

$$\lim_{|\mathbf{r}| \rightarrow \infty} \vec{\mathbf{G}}_s(\mathbf{r}, \mathbf{r}_k) = \frac{\exp(ik_j |\mathbf{r}|)}{|\mathbf{r}|} \vec{\mathbf{G}}_s^\infty(\mathbf{r}'_k, \mathbf{n}_r). \quad (2.18)$$

Here, \mathbf{r}'_k is the projection of \mathbf{r}_k on the surface of the layered structure and \mathbf{n}_r denotes the direction of observation (ϑ, φ) . When inserting Eq. (2.11) with the asymptotic forms of $\vec{\mathbf{G}}_o$ and $\vec{\mathbf{G}}_s$ into Eq. (2.16), the exponential terms which have been extracted out of the asymptotic values cancel out, and the dependence on radial distance reduces to $|\mathbf{r}|^{-2}$. The latter cancels out after inserting $\langle \mathbf{S} \rangle$ into Eq. (2.15). Hence, with Eqs. (2.15)–(2.18) the angular power density of a system with N dipoles can be written as

$$p(\vartheta, \varphi) = \frac{1}{2} \omega^4 \mu_o^2 \sqrt{\frac{\varepsilon_o \varepsilon_j}{\mu_o}} \left| \sum_{n=1}^N [\vec{\mathbf{G}}_o^\infty(\mathbf{r}_n, \mathbf{n}_r) + \vec{\mathbf{G}}_s^\infty(\mathbf{r}'_n, \mathbf{n}_r)] \mathbf{p}_n \right|^2. \quad (2.19)$$

This equation allows to determine the radiation patterns of an arbitrary number of coherently radiating dipoles. It will be used in the following for the separate integration of the light radiated into the upper half-space (P^\uparrow) and the light coupled into the substrate (P^\downarrow). The latter is further split into two contributions depending on the angle α of propagation. α denotes the angle enclosed by the direction of observation \mathbf{n}_r and the *negative* z axis. In this case, $\alpha_c = \arcsin(k_1/k_n)$ (k_1 and k_n are the wavenumbers of upper and lower half-spaces) defines the critical angle. Light radiated within α_c ($\alpha < \alpha_c$) is designated as *allowed* light and light radiated beyond α_c ($\alpha > \alpha_c$) is denoted as *forbidden* light.³⁸

III. RESULTS

The electromagnetic properties of the silver layer are described by a frequency dependent dielectric function $\varepsilon(\omega)$ [Fig. 2a], obtained from interpolated experimental data from Ref. 39. A glass substrate with a frequency independent

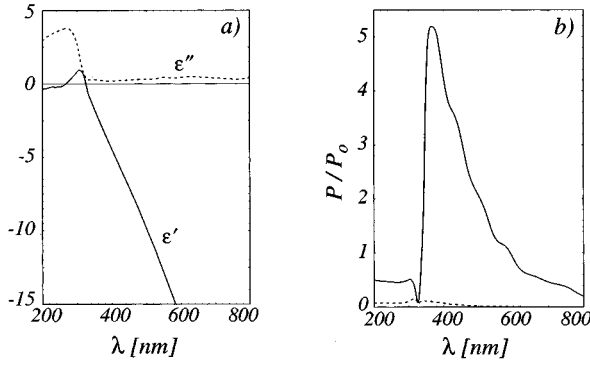


FIG. 2. (a) Interpolated dielectric function of silver according to Ref. 39. (b) Allowed (solid curve) and forbidden light (dashed curve) of a vertical electric dipole above a 50 nm silver layer vs. excitation wavelength λ . The curves are normalized with the total radiated power in free space, P_0 .

dielectric constant of $\epsilon_n = 2.25$ serves as mechanical support and the upper half-space is assumed to be vacuum $\epsilon_1 = 1$. The plasmon modes

$$k_{sp,\rho} = k'_{sp,\rho} + ik''_{sp,\rho} \quad (3.1)$$

are determined by the zeroes of the transcendental equation

$$1 + r_{1,2}^{(p)}(k_\rho) r_{2,3}^{(p)}(k_\rho) \exp(2ik_{z2}d) = 0, \quad (3.2)$$

where $r_{1,2}^{(p)}$ and $r_{2,3}^{(p)}$ are the Fresnel reflection coefficients for p polarized light of the upper (vacuum-silver) and lower (silver-glass) interface, respectively. The phase condition at the interfaces requires that the radial component of the wavenumber (k_ρ) is continuous. The vertical component in domain j is determined by the wavenumber $k_j = (\omega/c) \sqrt{\epsilon_j}$ and k_ρ according to

$$k_{jz} = \sqrt{k_j^2 - k_\rho^2} \text{ with } \text{Im}\{k_{jz}\} > 0. \quad (3.3)$$

The condition $\text{Im}\{k_{jz}\} > 0$ selects the solutions on one Riemann sheet and thus makes the square root single valued. The plasmon modes are dependent on the wavelength λ and the thickness d of the layer. $k'_{sp,\rho}$ determines the propagation constant of the surface plasmon, whereas $k''_{sp,\rho}$ determines its damping. For some λ and d , there are two distinct plasmon modes, one of which is bound to the upper interface and the other to the lower interface. For example, at $\lambda = 488$ nm and for $d = 50$ nm, the modes bound to the upper and lower interface have propagation constants of $k'_{sp,\rho} = 1.062k_1$ and $k'_{sp,\rho} = 1.75k_1$, respectively. The former mode shows a resonance at $\lambda = 370$ nm, where it reaches a value of $k'_{sp,\rho} = 1.225k_1$, and the latter has a resonance at $\lambda = 437.5$ nm, with a corresponding value of $k'_{sp,\rho} = 1.895k_1$. For large d the plasmon modes of the two interfaces become almost decoupled and the resulting two $k_{sp,\rho}$ values can be determined from the single interface conditions. Note that plasmon modes propagating on the interface metal-glass do not radiate. This is because the wavelengths of these plasmon modes are generally smaller than the wavelengths of the propagating waves in the two half spaces. Thus, far-field detection of surface plasmons is limited to the modes guided along the interface metal-vacuum. The dispersion of surface plasmons in presence of damping as well as the dependence on the layer thickness is rather

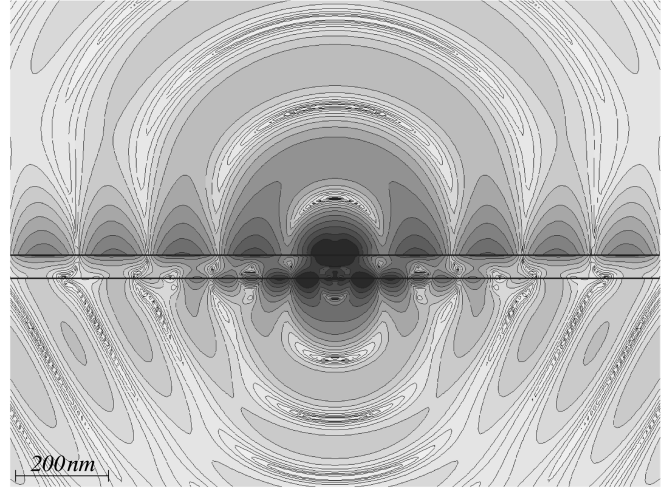


FIG. 3. Excitation of a surface plasmon wave by a horizontal electric dipole at $\lambda = 370$ nm. The dipole axis encloses an angle of 30° with the plane of the figure. The figure shows lines of constant power density (factor of 2 between successive contour lines) at a certain point of time. Silver layer: $\epsilon = -2.85 + i0.22$, $d = 50$ nm; upper half-space: $\epsilon_1 = 1$; lower half-space: $\epsilon_n = 2.25$.

complicated, as the existence of plasmon modes [solutions of Eq. (3.2)] is governed by a complex cutoff behavior.^{40,41}

Surface plasmons propagating along the surface of a metal layer of finite thickness radiate into a certain angle α_k (Kretschmann angle). This angle lies beyond the critical angle of total internal reflection

$$\alpha_c = \arcsin(k_1/k_n). \quad (3.4)$$

Beside dissipative losses in the metal layer, the radiative decay limits the lifetime of locally excited surface plasmons. On the other hand, it enables the detection (or excitation) of surface plasmons in the far-field. For too thin layers the plasmon modes are highly dissipative, i.e., $k''_{sp,\rho}$ has a large value, whereas for thick layers the coupling to far-field radiation is weak. For silver, an optimum was found near $d = 50$ nm. In Fig. 2(b) the spectrum of the allowed and the forbidden light are shown for $d = 50$ nm and for a vertically oriented electric dipole. The dip in the curves near $\lambda = 340$ nm corresponds to the bulk plasmon ($\epsilon \rightarrow 0$). The optimum excitation wavelength of the surface plasmon is found to be at $\lambda = 370$ nm.

The plasmon field at $\lambda = 370$ nm is shown in Fig. 3 for a 50 nm layer. At this wavelength the dielectric constant of silver is $\epsilon = -2.85 + i0.22$. The field is excited by a horizontal electric dipole with its axis enclosing an angle of 30° with the plane of the figure. For increasing distance from the dipole source, the figure shows how the plasmon field separates more and more from the spherical wave radiated into the upper half space. It is easy to show, that the cylindrical plasmon field is an independent solution of the wave equation. However, since this solution diverges along the cylindrical axis, the locally excited plasmon field must be coupled to other solutions close to the origin.⁴²

The wavelength of the surface plasmon ($\lambda^{(p)} = 2\pi/k'_{sp,\rho}$) is shorter than that of the spherical wave ($\lambda = 2\pi/k_1$). This implies that the plasmon can only be ex-

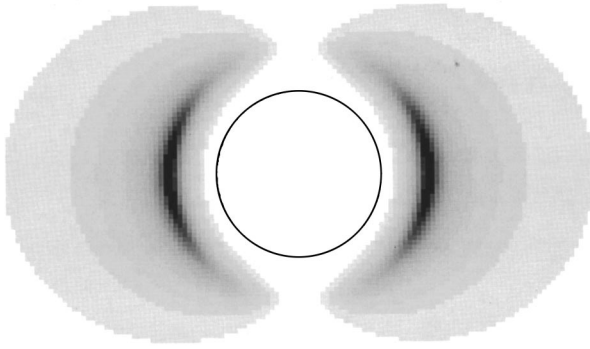


FIG. 4. Far-field intensity on a horizontal plane in the lower half-space. The configuration corresponds to Fig. 3. The circle indicates the critical angle $\alpha_c=41.81^\circ$ and the plasmon peaks are at $\alpha_k=54.75^\circ$.

cited by evanescent components of the source spectrum. In the lower medium the plasmon radiates predominantly into the well defined angle α_k given by

$$\alpha_k = \arcsin(k'_{sp,p}/k_n), \quad (3.5)$$

where $k_n = (\omega/c)\sqrt{\epsilon_n}$ is the wavenumber of the substrate. The angular width of the radiation is determined by $k''_{sp,p}$. The propagation constant of the surface plasmon is $k'_{sp,p} = 1.225k_1$ corresponding to an angle $\alpha_k = 54.75^\circ$. The critical angle is $\alpha_c = 41.81^\circ$. Fig. 4 shows the far-field intensity on a horizontal plane. This image would result by collecting the radiation with a high numeric aperture lens and projecting it on a photographic plate. The spherical wave

radiated in forward direction is much weaker than the plasmon peaks and therefore cannot be seen in the image. For a visible Ar^+ wavelength of $\lambda = 488 \text{ nm}$, the plasmon wavelength becomes larger ($k'_{sp,p} = 1.062k_1$) and the Kretschmann angle shifts closer to the critical angle ($\alpha_k = 45.07^\circ$). Fig. 5(a) presents the radiation pattern for the situation shown in Fig. 3. The pattern is entirely dominated by the plasmon peaks beyond the critical angle. The angular distribution of the far-field intensity is shown on a smaller angular range in Fig. 5(b) for the two wavelengths $\lambda = 488 \text{ nm}$ and $\lambda = 514.5 \text{ nm}$. Here, in order to correspond with a given experimental set-up, the dielectric constant of the substrate is $\epsilon_n = 2.31$. The width of the peaks is $\approx 1.5^\circ$. Fig. 5(c) shows schematically the excitation of surface plasmons by means of the ATR technique. A p polarized plane wave incident from the denser medium hits the silver layer and the intensity of the reflected wave is recorded in the far-field as a function of the incident angle α . At the angle α_k , where the parallel k vector of the incident wave matches with $k_{sp,p}$ of the surface plasmon, the reflected wave has a minimum. Consequently, most of the energy is coupled to the surface plasmon [Fig. 5(d)]. Thus, in some way, the ATR configuration is reciprocal to the configuration of local excitation.

The surface plasmons of a vertical electric dipole are rotationally symmetric with respect to the dipole axis, whereas they have a $\cos\varphi$ symmetry for a horizontally oriented dipole. On the other hand, a vertical magnetic dipole cannot couple to surface plasmons, since its k spectrum has

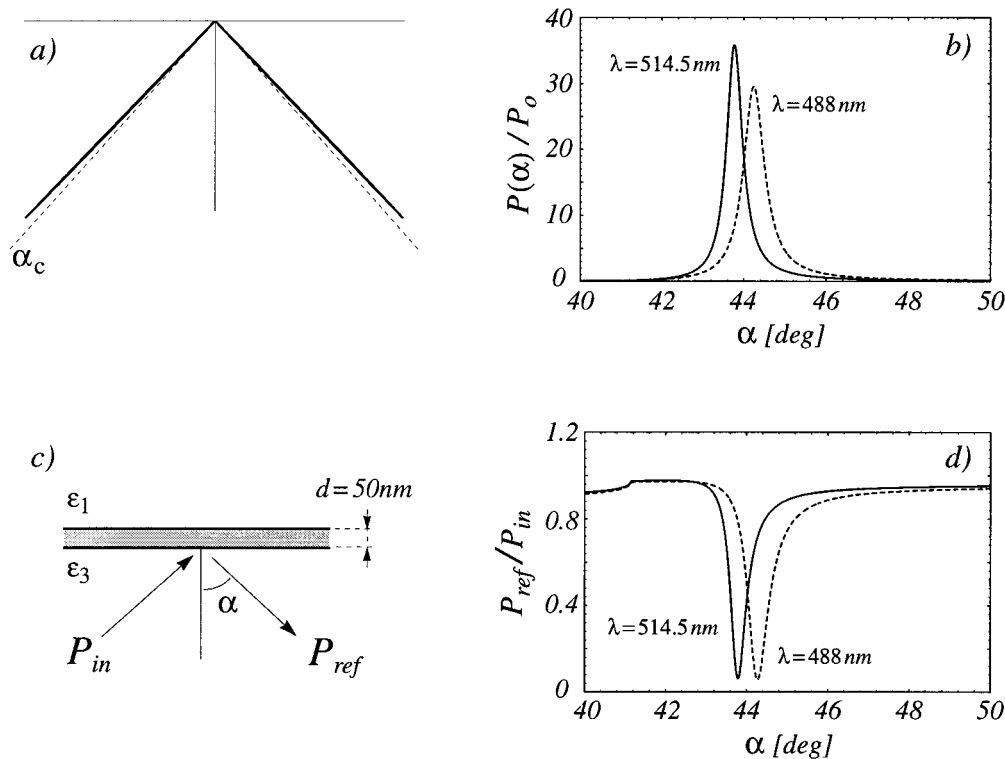


FIG. 5. (a) Radiation pattern corresponding to the situation in Fig. 3 but for $\lambda = 488 \text{ nm}$ and $\epsilon_n = 2.25$. α_c indicates the critical angle. (b) Angular far-field intensity for two different excitation wavelengths. The curves are normalized by the corresponding total radiation P_o in free space. (c) Principle of the ATR technique. (d) Ratio of the reflected intensity to the incident intensity as a function of the angle of incidence. Same geometry as in (b). For all figures the lower medium has a dielectric constant of $\epsilon_n = 2.31$.

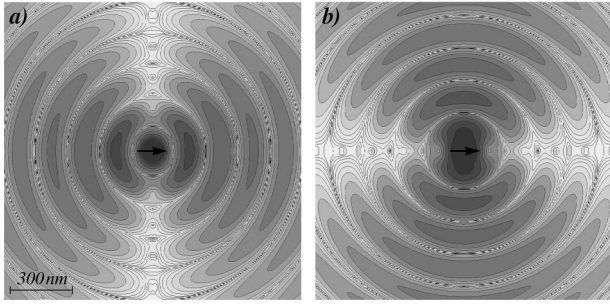


FIG. 6. Surface plasmon fields at $\lambda = 370$ nm evaluated on the surface of the silver layer. Excitation by a horizontal electric dipole (a) and by a horizontal magnetic dipole (b). The dipole axes point from left to right. The figures show lines of constant power density (factor of 2 between successive contour lines) at a certain point of time. Silver layer: $\epsilon = -2.85 + i0.22$, $d = 50$ nm; upper half-space: $\epsilon = 1$; lower half-space: $\epsilon = 2.25$.

no p polarized components, i.e., the \mathbf{E} field is always parallel to the interfaces and no surface charge accumulation can be established. This does not hold for the horizontal magnetic dipole, where the excited surface plasmons also have a $\cos\varphi$ symmetry. The surface plasmons of a horizontal electric dipole propagate predominantly in the direction of the dipole axis, whereas for a horizontal magnetic dipole they propagate perpendicular to its axis. The resulting intensities on the surface of the Ag layer are depicted in Fig. 6. The reason for this different behavior lies in the different \mathbf{E} field distribution of the two dipoles. The plasmon field is established by the *evanescent* \mathbf{E} field components that are perpendicular to the interfaces. For the horizontal electric dipole these components dominate in the direction of the dipole axis, whereas they completely vanish perpendicular to it. The exact opposite situation applies to the horizontal magnetic dipole (Fig. 4).

So far, a single dipole with a fixed dipole moment has been used to excite surface plasmons on a finite silver layer, and no coupling between the dipole and its environment has been taken into account. However, if the dipole is induced by external fields, a polarizability $\tilde{\alpha}_k(\omega)$ has to be introduced relating the induced moment \mathbf{p}_k to the local field [Eq. (2.9)]. The explicit form of $\tilde{\alpha}_k(\omega)$ is given by Eq. (2.12). It depends on the third power of the particle's radius and shows a resonance for $\epsilon_k(\omega) \rightarrow -2\epsilon_1$, where ϵ_k is the dielectric constant of the particle. This condition corresponds to the particle's surface plasmon resonance.³⁵ With regard to the experimental situation in aperture SNOM, surface plasmon interactions have been studied for the system depicted in Fig. 1. In this configuration a light emitting optical probe is scanned over several protrusions located on the surface of the silver layer. Both, probe and protrusions, are represented by spherical particles of different size. The particle that represents the optical probe is locally excited by the field \mathbf{E}_o and illuminates the system with its resulting dipolar field. Different to the experimental situation, the probe is not retracted when coming close to a protruding particle. Therefore, the probe penetrates through the protrusions and the results are not valid very close to the protruding particles.

For every position of the probe, the self-consistent dipole moments have to be determined by using Eq. (2.10)

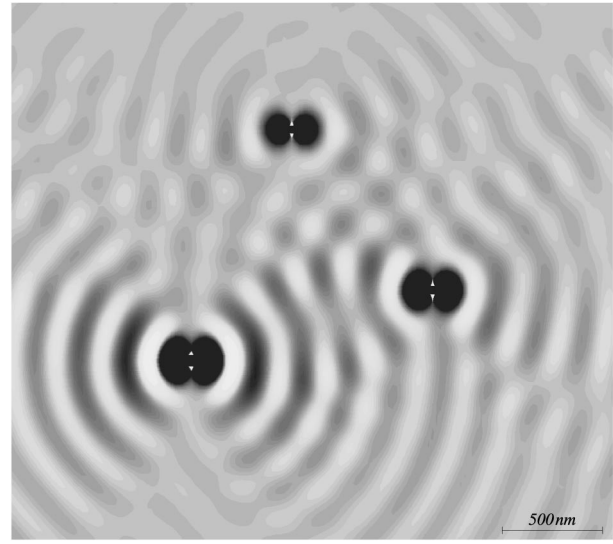


FIG. 7. Forbidden light scan image for the configuration shown in Fig. 1.

with Green's dyadic of the layered reference system (Appendix A). For time harmonic excitation, the dipole moment \mathbf{p} of a certain particle rotates on an ellipse, and is therefore entirely determined by the two components of \mathbf{p} lying in the plane of the ellipse. But since the plane of the ellipse is not a priori known, a third component is needed. Once the dipole moments are determined, the resulting field distribution as well as the far-fields can be computed according to Eq. (2.19). Fig. 7 shows the *forbidden light* scan image that results from numerically integrating the power density over the forbidden regime. For every position of the probe the resulting value is assigned to the momentary coordinates of the probe.

At a fixed position, the probe excites a surface plasmon propagating along the layer and being scattered by the protrusions. This primary surface plasmon field, together with the direct radiation of the probe induce dipoles in the protruding particles. These dipoles excite secondary plasmon fields. The resulting field on the surface of the layer is therefore a superposition of individual surface plasmon fields, and the light observed at the Kretschmann angle α_k depends on the phase relations between the individual fields. The resulting plasmon-interference image depends on the height of the probe and on the size of the protruding particles: For increasing particle size, the distance of the induced dipole to the surface of the layer increases and the less evanescent components reach the surface. The coupling to surface plasmons should therefore exponentially depend on the particle's diameter. On the other hand, the strength of an induced dipole increases with the third power of its radius predicting a stronger coupling for large particles. For the particles shown in Fig. 7, the latter has been the dominating factor, i.e., the larger the particle, the stronger the induced dipole field. Notice that a given particle has also an influence on itself: the own field that arrives at the particle after being reflected at the surface of the layer tends to enhance its dipole moment the closer the particle comes to the surface. However, almost the same results have been obtained when $\tilde{\mathbf{G}}_s(\mathbf{r}_k, \mathbf{r}_k)$ in Eq.

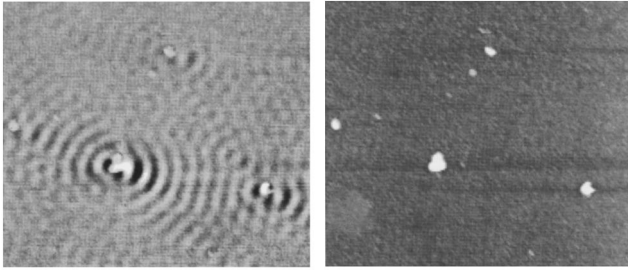


FIG. 8. Experimental images recorded with aperture SNOM (see Ref. 43). Forbidden light scan image (left) and shear-force scan image (right). The parameters of the layered reference system correspond to those of the theoretical model.

(2.10) was ignored indicating that this interaction is weak.

If the probe particle is close to the surface, its primary surface plasmon field will dominate and the resulting interference pattern will be weaker. On the other hand, the probe particle will not be able to excite any primary surface plasmon field at greater distances from the surface. Hence, there must be an optimum height for which the secondary plasmons are excited not only by the primary plasmon field but also by the direct radiation of the optical probe.

Fig. 8 shows experimental images of a similar configuration recorded with aperture SNOM.⁴³ The figure on the left hand side shows the forbidden light image whereas the other figure presents the simultaneously recorded shear-force image.⁴⁴ The bright spots on the latter represent protrusions of different sizes. The experimental and theoretical forbidden light images are in excellent accordance with each other. Even the contrast of the two images is in approximate correspondence. In the experimental image, the polarization of the exciting light is slightly twisted compared with the theoretical image. The main deviation is found for the centers of the particles, where the theoretical image is not valid since the optical probe has not been retracted.

The *allowed light* images which are not shown here, also exhibit interference undulations. These undulations are caused by phase differences between the induced dipoles and are determined by both, the primary plasmon fields and the primary radiation fields. However, the undulations are much weaker compared with those observed for the forbidden light and the resulting patterns depend strongly on the conditions, such as scanning height, layer thickness, and configuration of the particles. In some cases, the allowed images show hyperbola shaped patterns similar to those in Refs. 43,45.

In order to prove that the interference patterns in the forbidden light images are indeed plasmon interferences, the same structure has been imaged with a smaller excitation wavelength $\lambda = 370$ nm. As discussed above, the coupling to surface plasmons is strongest for this wavelength and the plasmon wavelength can be well separated from the exciting wavelength ($\lambda_{(p)} = \lambda/1.225 = 302$ nm). For this configuration, Fig. 9 shows the allowed light, the forbidden light, and the light scattered into the upper half space along a single scan trace. The estimated periodicities are approximately 160, 150, and 180 nm, respectively. The periodicity of the forbidden light matches well with $\lambda_{(p)}/2$, whereas the light scattered into the upper half space shows a periodicity close

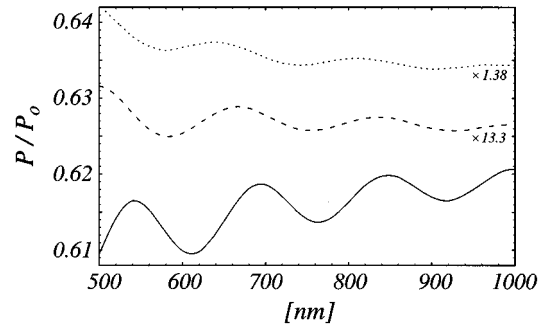


FIG. 9. Forbidden light (solid curve), allowed light (dashed curve) and light scattered into the upper half space (dotted curve) for a single scan trace at $\lambda = 370$ nm. The scan trace is recorded to the left of particle *B* in Fig. 1. The parameters are the same as in Fig. 1 but with $\epsilon_{Ag} = -2.85 + i0.22$.

to $\lambda/2$. Thus, in this example, the phase differences between the individual dipole moments seem to be dominated by the direct radiation of the source and not by the primary plasmon field. The periodicity of the allowed light is between $\lambda_{(p)}/2$ and $\lambda/2$ suggesting that also the primary plasmon field contributes to phase differences.

IV. CONCLUSIONS

Coupling mechanisms between surface plasmon waves and their far-field radiation have been discussed. The theoretical analysis is based on a coupled dipole formalism that uses Green's functions of a layered reference system. Because of the long range interactions of surface plasmon waves, it is neither possible to neglect retardation nor it is possible to limit the lateral size of the layered reference system. Instead, this application requires an efficient and accurate calculation of the dyadic Green's functions. The optical probe as well as the protruding particles have been modeled as single dipolar centers in order to reduce the discussion on a basic level. Larger objects with arbitrary shape can be calculated in the same way by simply dividing the objects into a number of dipolar cells.⁴⁶⁻⁴⁸ It has been shown that surface plasmon interactions can be probed in the far-field by recording the forbidden light.

ACKNOWLEDGMENTS

The authors thank Ch. Hafner and J. Waldvogel for stimulating discussions. The work has been supported in part by the Swiss National Science Foundation.

APPENDIX A: DYADIC GREEN'S FUNCTION OF A PLANARLY LAYERED REFERENCE SYSTEM

The dyadic Green's function $\vec{\mathbf{G}}(\mathbf{r}, \mathbf{r}_k)$ represents the electric field $\mathbf{E}(\mathbf{r})$ for the three major orientations of a dipole \mathbf{p}_k located at \mathbf{r}_k according to

$$\mathbf{E}(\mathbf{r}) = \omega^2 \mu_o \vec{\mathbf{G}}(\mathbf{r}, \mathbf{r}_k) \mathbf{p}_k. \quad (\text{A1})$$

The components of $\vec{\mathbf{G}}$ are therefore determined by the fields of an arbitrarily oriented dipole embedded in a planarly layered reference system. A cylindrical coordinate system is chosen with the z axis perpendicular to the interfaces and

with $z=0$ denoting the topmost interface. The x axis and the y axis are defined by $\varphi=0$ and $\varphi=\pi/2$, respectively. The radius ρ corresponds to $(x^2+y^2)^{-1/2}$ and the overall thickness of the layered system is denoted by δ . It is assumed that the dipole is located in the *upper* half-space at $\mathbf{r}_k=(x,y,z)=(0,0,h)$. Since the primary part $\vec{\mathbf{G}}_o$ can be found in many textbooks, only the results for $\vec{\mathbf{G}}_s$ are discussed, i.e., the primary part is suppressed. Furthermore, in order not to focus on a system with a certain number of layers, the solutions are given in general form for the upper ($j=1$) and lower ($j=n$) half-spaces in terms of the reflection ($r^{(s)}, r^{(p)}$) and transmission ($t^{(s)}, t^{(p)}$) coefficients of the

entire structure. Therein, the indices (s) and (p) denote s and p polarization, respectively. The wavevector \mathbf{k}_j in domain j is decomposed into a vertical and a parallel component according to

$$k_{jz} = \sqrt{k_j^2 - k_\rho^2} \quad \text{with } \text{Im}\{k_{jz}\} > 0. \quad (\text{A2})$$

The curves $\text{Im}\{k_{jz}\}=0$ define branch cuts in the complex k_ρ plane. In order to stay on the proper Riemann sheet the branch cuts may not be trespassed by the path of integration.

With the definitions above, $\vec{\mathbf{G}}_s$ in cartesian components becomes

$$\vec{\mathbf{G}}_s(\mathbf{r}, \mathbf{r}_k) = \frac{1}{4\pi k_1} \begin{pmatrix} \cos^2 \varphi G_1 - \sin^2 \varphi G_2 & \sin \varphi \cos \varphi [G_1 + G_2] & \cos \varphi G_4 \\ \sin \varphi \cos \varphi [G_1 + G_2] & \sin^2 \varphi G_1 - \cos^2 \varphi G_2 & \sin \varphi G_4 \\ \cos \varphi G_3 & \sin \varphi G_3 & G_5 \end{pmatrix}$$

where the terms G_i are Sommerfeld type integrals which have to be evaluated numerically for accurate results. If the following abbreviations are used for the Bessel functions

$$J_0 = J_0(k_\rho \rho), \quad J'_0 = -J_1(k_\rho \rho) \quad \text{and} \\ J''_0 = \frac{1}{k_\rho \rho} J_1(k_\rho \rho) - J_0(k_\rho \rho), \quad (\text{A3})$$

the terms G_i in the *upper half-space* read

$$G_1 = i \int_0^\infty dk_\rho \exp[ik_{1z}(z+h)] \left(J''_0 k_\rho k_{1z} r^{(p)} - \frac{J'_0}{\rho} \frac{k_1^2}{k_{1z}} r^{(s)} \right), \quad (\text{A4})$$

$$G_2 = -i \int_0^\infty dk_\rho \exp[ik_{1z}(z+h)] \left(\frac{J'_0}{\rho} k_{1z} r^{(p)} - J''_0 k_\rho \frac{k_1^2}{k_{1z}} r^{(s)} \right), \quad (\text{A5})$$

$$G_3 = \int_0^\infty dk_\rho \exp[ik_{1z}(z+h)] J'_0 k_\rho^2 r^{(p)}, \quad (\text{A6})$$

$$G_4 = - \int_0^\infty dk_\rho J_0 k_\rho^2 r^{(p)} \exp[ik_{1z}(z+h)], \quad (\text{A7})$$

$$G_5 = i \int_0^\infty dk_\rho J_0 \frac{k_\rho^3}{k_{1z}} r^{(p)} \exp[ik_{1z}(z+h)], \quad (\text{A8})$$

whereas in the *lower half-space* they are determined by

$$G_1 = -i \int_0^\infty dk_\rho \exp\{i[k_{1z}h - k_{nz}(z+\delta)]\} \\ \times \left(J''_0 k_\rho k_{nz} \frac{\varepsilon_1}{\varepsilon_n} t^{(p)} + \frac{J'_0}{\rho} \frac{k_1^2}{k_{1z}} t^{(s)} \right), \quad (\text{A9})$$

$$G_2 = i \int_0^\infty dk_\rho \exp\{i[k_{1z}h - k_{nz}(z+\delta)]\} \left(\frac{J'_0}{\rho} k_{nz} \frac{\varepsilon_1}{\varepsilon_n} t^{(p)} + J''_0 k_\rho \frac{k_1^2}{k_{1z}} t^{(s)} \right), \quad (\text{A10})$$

$$G_3 = i \int_0^\infty dk_\rho \exp\{i[k_{1z}h - k_{nz}(z+\delta)]\} J'_0 k_\rho^2 \frac{\varepsilon_1}{\varepsilon_n} t^{(p)}, \quad (\text{A11})$$

$$G_4 = \frac{k_1}{k_n} \int_0^\infty dk_\rho J_0 k_\rho^2 \frac{k_{nz}}{k_{1z}} t^{(p)} \exp\{i[k_{1z}h - k_{nz}(z+\delta)]\}, \quad (\text{A12})$$

$$G_5 = i \int_0^\infty dk_\rho J_0 \frac{k_\rho^3}{k_{1z}} t^{(p)} \exp\{i[k_{1z}h - k_{nz}(z+\delta)]\}. \quad (\text{A13})$$

In the expressions above, the location of the dipole is $\mathbf{r}_k=(0,0,h)$, whereas the point of observation is given by $\mathbf{r}=(\rho, \varphi, z)$. Note that the reflection and transmission coefficients refer to the entire layered structure. They can be recursively generated from the Fresnel reflection and transmission coefficients of the individual interfaces.^{30,49} As an example, the reflection and transmission coefficients of a single layer of thickness d read

$$r^{(p,s)} = \frac{r_{1,2}^{(p,s)} + r_{2,3}^{(p,s)} \exp(2ik_{2z}d)}{1 + r_{1,2}^{(p,s)} r_{2,3}^{(p,s)} \exp(2ik_{2z}d)} \quad (\text{A14})$$

$$t^{(p,s)} = \frac{t_{1,2}^{(p,s)} t_{2,3}^{(p,s)} \exp(ik_{2z}d)}{1 + r_{1,2}^{(p,s)} r_{2,3}^{(p,s)} \exp(2ik_{2z}d)}, \quad (\text{A15})$$

where $r_{i,j}^{(p,s)}$ and $t_{i,j}^{(p,s)}$ are the reflection and transmission coefficients of the interface (i,j) .⁵⁰

¹H. Haken, in *Quantum Field Theory of Solids* (North Holland, Amsterdam, 1976), Chap. 27.

- ² *Electromagnetic Surface Modes*, edited by A. D. Boardman (Wiley, Chichester, 1982).
- ³ J. R. Sambles and R. A. Innes, *Surface Plasmon-Polaritons*, Vol. 9 of *IOP Short Meetings, Series* (Institute of Physics and Physical Society, Bristol, 1987), pp. 121–138.
- ⁴ R. W. Alexander, R. J. Bell, and C. A. Ward, in *Electromagnetic Surface Modes*, edited by A. D. Boardman (Wiley, Chichester, 1982), pp. 201–217.
- ⁵ R. H. Ritchie, *Phys. Rev.* **106**, 874 (1957).
- ⁶ T. Kloos, *Z. Phys.* **208**, 77 (1968).
- ⁷ A. Otto and J. B. Swan, *Z. Phys.* **206**, 277 (1967).
- ⁸ A. Bagchi and C. B. Duke, *Phys. Rev. B* **5**, 2784 (1972).
- ⁹ H. R  ther, *Surface Plasmons*, Vol. 111 of *Springer Tracts in Modern Physics* (Springer, Berlin, 1988).
- ¹⁰ A. Otto, *Z. Phys.* **216**, 398 (1968).
- ¹¹ E. Kretschmann and H. Raether, *Z. Naturforsch.* **23a**, 2135 (1968).
- ¹² K. Welford, *Surface Plasmon-Polaritons*, Vol. 9 of *IOP Short Meetings, Series* (Institute of Physics and Physical Society, Bristol, 1987), pp. 25–99.
- ¹³ G. W. Ford and W. H. Weber, *Physics Reports* **113**, 195 (1984).
- ¹⁴ E. T. Arakawa, M. W. Williams, R. N. Hamm, and R. H. Ritchie, *Phys. Rev. Lett.* **31**, 1127 (1973).
- ¹⁵ U. C. Fischer and D. W. Pohl, *Phys. Rev. Lett.* **62**, 458 (1989).
- ¹⁶ M. Specht, J. D. Pedarnig, W. M. Heckl, and T. W. H  nsch, *Phys. Rev. Lett.* **68**, 476 (1992).
- ¹⁷ T. J. Silva, S. Schultz, and D. Weller, *Appl. Phys. Lett.* **65**, 658 (1994).
- ¹⁸ T. Takemori, M. Inoue, and K. Ohtaka, *J. Phys. Soc. Jpn.* **56**, 1587 (1987).
- ¹⁹ C. Girard, *Appl. Opt.* **31**, 5380 (1992).
- ²⁰ C. Girard, X. Bouju, and A. Dereux, in *Near Field Optics*, Vol. 242 of *NATO Advanced Study Institute, Series E*, edited by D. W. Pohl and D. Courjon (Kluwer Academic, Dordrecht, 1993), pp. 199–208.
- ²¹ P. K. Aravind and H. Metiu, *Surf. Sci.* **124**, 506 (1983).
- ²² O. Keller, M. Xiao, and S. Bozhevolnyi, *Surf. Sci.* **280**, 217 (1993).
- ²³ M. Meier, A. Wokaun, and P. F. Liao, *J. Opt. Soc. Am.* **2**, 931 (1985).
- ²⁴ F. Pincemin, A. A. Maradudin, A. D. Boardman, and J. J. Greffet, *Phys. Rev. B* **50**, 15261 (1994).
- ²⁵ D. W. Pohl, W. Denk, and M. Lanz, *Appl. Phys. Lett.* **44**, 651 (1984).
- ²⁶ E. Betzig and J. K. Trautman, *Science* **257**, 189 (1992).
- ²⁷ H. Heinzelmann and D. W. Pohl, *Appl. Phys. A* **59**, 89 (1994).
- ²⁸ L. Novotny and D. W. Pohl, in *Photons and Local Probes*, *NATO Advanced Study Institute, Series E*, edited by O. Marti and R. M  ller (Kluwer Academic, Dordrecht, 1995), pp. 21–33.
- ²⁹ J. J. H. Wang, *Generalized Moment Methods in Electromagnetics* (Wiley, Chichester, 1991).
- ³⁰ W. C. Chew, *Waves and Fields in Inhomogeneous Media*, 1st ed. (Van Nostrand Reinhold, New York, 1990).
- ³¹ A. D. McLachlan, *Mol. Phys.* **34**, 381 (1964).
- ³² A. D. Yaghjian, *Proc. IEEE* **68**, 248 (1980).
- ³³ J. V. Bladel, *IRE Trans. Antennas Propagat.* **9**, 563 (1961).
- ³⁴ A. Lakhtakia, *J. Mod. Phys. C* **3**, 583 (1992).
- ³⁵ C. F. Bohren and D. R. Huffmann, *Absorption and Scattering of Light by Small Particles* (Wiley, New York, 1983).
- ³⁶ B. T. Draine, *Astrophys. J.* **333**, 848 (1988).
- ³⁷ L. Novotny, *J. Opt. Soc. Am. A*, in press (1997).
- ³⁸ B. Hecht, D. W. Pohl, H. Heinzelmann, and L. Novotny, in *Photons and Local Probes*, *NATO Advanced Study Institute, Series E*, edited by O. Marti and R. M  ller (Kluwer, Dordrecht, 1995), pp. 93–107.
- ³⁹ P. B. Johnson and R. W. Christy, *Phys. Rev. B* **6**, 4370 (1972).
- ⁴⁰ B. Prade, J. Y. Vinet, and A. Myszyrowicz, *Phys. Rev. B* **44**, 13 556 (1991).
- ⁴¹ L. Novotny and C. Hafner, *Phys. Rev. E* **50**, 4094 (1994).
- ⁴² P. S. Epstein, *Proc. Natl. Acad. Sci. USA* **33**, 195 (1947).
- ⁴³ B. Hecht, H. Bielefeldt, L. Novotny, Y. Inouye, and D. W. Pohl, *Phys. Rev. Lett.* **77**, 1889 (1996).
- ⁴⁴ R. Toledo-Crow, P. C. Yang, Y. Chen, and M. Vaez-Iravani, *Appl. Phys. Lett.* **60**, 2957 (1992).
- ⁴⁵ M. H. P. Moers, ISBN 90-9008593-9, University of Twente, The Netherlands, CIP-Gegevens Koninklijke Bibliotheek, Den Haag, 1995.
- ⁴⁶ O. J. F. Martin, A. Dereux, and C. Girard, *J. Opt. Soc. Am. A* **11**, 1073 (1994).
- ⁴⁷ R. Carminati and J. J. Greffet, *J. Opt. Soc. Am. A* **12**, 2716 (1995).
- ⁴⁸ M. A. Taubenblatt and T. K. Tran, *J. Opt. Soc. Am. A* **10**, 912 (1993).
- ⁴⁹ L. M. Brekhovskikh, *Waves in Layered Media*, 2nd ed. (Academic, New York, 1980).
- ⁵⁰ M. Born and E. Wolf, *Principles of Optics*, 6th ed. (Pergamon, Oxford, 1970).